A Novel Multi-Degree-of-Freedom Thick-Film Ultrasonic Motor

Manaba Aoyagi, Steve P. Beeby, and Neil M. White

Abstract—**This paper describes a new multi-degree-of-freedom (MDOF) ultrasonic motor that comprises few parts and is based on low-cost thick-film technology. Conventional ultrasonic motors using bulk lead zirconate titanate (PZT) or thin-film PZT layers are relatively expensive at the present time. Thick-film printed PZT technology provides the opportunity to reduce the costs of ultrasonic motors. To demonstrate the feasibility of this approach, an ultrasonic motor was fabricated from alumina using thick-film printed PZT actuators. The thick-film PZT and electrode layers were printed on a thin alumina plate, and a tiny cylinder was mounted at its center. This cylinder magnifies the lateral displacement of the stator, holds the spherical rotor, and transmits the driving force to the sphere. Three bending vibrations, B_{22}, B_{30}, B_{03}, of the plate were applied to rotate the sphere. Sufficient displacements for rotating the sphere were obtained near the resonance of B_{22} by applying an excitation voltage of 200 V peak-to-peak via a three-phase drive circuit. Rotations in three orthogonal directions have been observed by controlling the phase of the driving signal to the PZT electrodes, and a MDOF ultrasonic motor was successfully realized.**

I. Introduction

Recently, both ultrasonic motors and piezoelectric actuators have been applied to many practical industrial applications. Some of these have been miniaturized into millimeter-sized devices and have been used, for example, in wrist watches [1]. These devices typically use bulk PZT ceramic plates, which exhibit high levels of piezoelectric activity and can generate large forces from moderate applied electric fields. Bulk ceramic PZT is, in its simplest forms (such as discs and plates), relatively inexpensive, although more elaborate shapes require more sophisticated processing and are therefore more expensive. Bulk ceramics must also be individually glued in place, and this extra processing also leads to increased costs. A lower cost method for producing piezoelectric actuators in a wide range of geometries for industrial requirements is particularly desirable.

An alternative approach to using bulk piezoceramics is either thin or thick-film technology. Materials deposited using thin-film techniques exhibit high levels of piezoelectric activity, but the thickness is limited to a few microns. In addition, their deposition processes, being typically sputtering [2], sol-gel [3], or hydrothermal [4] techniques, are rather expensive. Thick films are based on standard screen printing technology, which has been widely used within the microelectronics industry for many years. It can produce thicker layers than thin-film deposition methods. Therefore thick-film printed PZT layers are capable of generating larger actuating forces than thin-film layers. An example of the use of a thick-film piezoelectric layer as an actuator is the silicon micropump described by Koch *et al.* [5]. An additional advantage of the thick-film approach is that it is possible to fabricate a complete ceramic structure without the need for adhesives to attach the various parts.

Traditional composite vibrators are fabricated by fixing bulk piezoelectric ceramics to metal structures using adhesives. The difference in thermal expansion coefficients results in thermal stress within the composite. Ceramic materials have lower thermal expansion coefficients than metals (typically 6 ppm/°C for ceramics; greater than 15 ppm/°C for metals) [6]. Therefore, the device described here, based wholly on ceramics, will not suffer from the high levels of thermally induced stress often experienced in traditional composite vibrators. It should be noted, however, that the upper temperature limit for operating our device is limited by the Curie temperature of the piezoceramic material (typically 190°C).

In general, ultrasonic motors can achieve two-dimensional linear motion, in addition to reversible rotary motion, in a single device [7]. This can be achieved by carefully designing the shape of the vibrator and by exciting the correct vibration modes [8]. This point has been illustrated by other researchers [9], [10], who have developed a MDOF ultrasonic motor capable of actuating in many directions.

This paper describes a new type of MDOF ultrasonic motor fabricated on an alumina substrate with thick-film PZT layers printed on its surface. The feasibility of producing an ultrasonic motor using printed PZT layers is demonstrated through the development of the MDOF ultrasonic motor constructed wholly of ceramic. There are many potential applications for this type of ultrasonic motor, including micro robots and optical devices.

Manuscript received November 21, 2000; accepted July 23, 2001. The authors acknowledge the UK Engineering and Physical Sciences Research Council for funding a ROPA project (GRL 73906), which made this work possible.

M. Aoyagi is with the Department of Electrical Engineering, Yamagata University, Japan.

S. P. Beeby and N. W. White are with the Department of Electronics and Computer Science, University of Southampton, United Kingdom (e-mail: spb@ecs.soton.ac.uk).

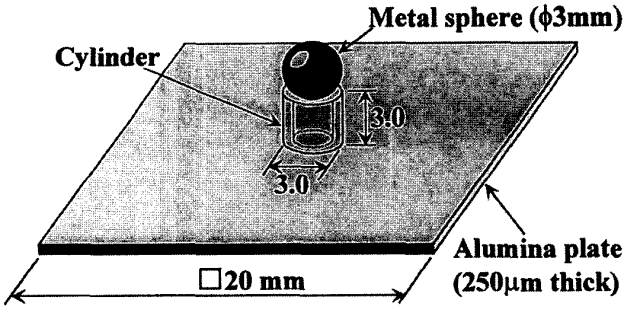

Fig. 1. Schematic of MDOF ultrasonic motor.

II. Operating Principle of MDOF Ultrasonic Motor

In general, an ultrasonic motor needs at least two vibration modes to form an elliptical displacement motion on the surface in contact with a rotor. Even single-phase drive ultrasonic motors consist of two vibration modes, which must be coupled to each other. All MDOF ultrasonic motors have advanced functionality compared with traditional single-degree-of-freedom (SDOF) ultrasonic motors. To achieve rotation around three orthogonal axes in the Cartesian coordinate system requires at least three resonant modes of which each displacement must be orthogonal to each other. The combination of various vibration modes has already been considered and demonstrated in MDOF ultrasonic motors [9], [10]. The MDOF ultrasonic motor proposed here is based on three bending resonance modes of a thin alumina square plate. The motor has been designed such that these modes are excited by thick-film printed PZT actuators.

A. Combination of Resonant Modes

The stator of the ultrasonic motor consists of a 20-mm square alumina plate, 250 μm thick with an alumina cylinder, 3 mm outside diameter, 0.5 mm thick and 3 mm long, attached to the center of the plate. This serves to amplify the lateral displacements of the plate associated with the bending modes, which, on the surface of the plate, are quite small. The alumina cylinder also holds a small metal sphere that serves as the rotor at the center of the vibrator. The thick-film PZT electrodes were printed on the underside of the alumina plate. A schematic of the motor is shown in Fig. 1.

The stator vibrator achieves the desired displacement of the rotor by generating both a rotary force and a vertical force (or thrust) that controls the surface friction between the vibrator and rotor. The rotary force and thrust are obtained by exciting the alumina plate into the correct mode of vibration. In this study, as a trial, the B_{30}, B_{03}, and B_{22} modes of the square plate, as illustrated in Fig. 2, were chosen. To illustrate the possible displacements, the deflections of a vertical bar located at the center of the plate are shown in Fig. 2. This bar simulates the displacements of the cylinder used in the actual device. Both B_{30} and B_{03} modes generate moments and swing the bar; the B_{22} mode produces a displacement in the direction perpendicular to the surface of the plate and, hence, shakes the bar vertically. Rotations around the x-axis, y-axis, and z-axis can be obtained by choosing a combination of resonant modes as shown in the boxed inserts in Fig. 2. When the B_{22} and B_{30} modes are excited by two phases, an elliptical displacement motion occurs at the end of the bar. Therefore, a sphere located at the center of the substrate will rotate around the x-axis parallel to the direction of the moment vector. When the B_{03} mode is combined with the B_{22} mode in place of the B_{30} mode, the rotor has rotation axis around the y-axis, because it is the orthogonal and symmetric mode of B_{30}. Moreover, the combination of the B_{30} and B_{03} modes causes a mode rotation [11]. The vector product of the direction vector moments of these modes generates a rotary force around the z-axis at the center of the plate. The axis of rotation can be changed, and the direction of rotation is reversible by switching the phase of the drive signal. Finally, the B_{22} mode has four nodal lines as shown in Fig. 2(a). These nodal lines cross each other at a point located very close to the nodal lines associated with the $B_{30}(B_{03})$ modes [Fig. 2(b and c)]. Hence, this motor can be supported at the crossing points of the four nodal lines of B_{22} mode with minimal vibration damping.

B. Modal Analyses

A finite element modal analysis (using a modified version of the SAP IV package) was used to simulate the structure to determine its resonant frequencies and associated mode shapes and to confirm the feasibility of the design. Fig. 3 shows some displacement plots from this simulation. Fig. 3(a) shows the B_{22} mode, Fig. 3(b) shows the B_{30} mode, and Fig. 3(c) shows the B_{03} mode. The B_{30} and B_{03} modes are orthogonal to each other and, because of their symmetrical shape, have the same resonance frequency. In these modes, the central cylinder is pushed upward and, because of the angular displacement of the plate, the tip of the cylinder is displaced laterally. Hence, the lateral displacements of the plate are magnified as expected. The resonance frequencies of the B_{30} (B_{03}) and B_{22} modes were 14.47 and 16.49 kHz, respectively. These frequencies should ideally be the same to reduce both mechanical and, as a result, electrical impedance. This improves the motor performance. In this case, however, the difference between these modes is not prohibitively large, and there is no other mode occurring between the B_{30} (B_{03}) and the B_{22} modes.

From the finite element analysis results and given previous work on degenerate-mode ultrasonic motors with nonequal resonant frequencies [8], a degree of confidence was established that these resonant modes can be simultaneously excited at the same frequency. Indeed, that type of ultrasonic motor still works well, especially if the resonant frequencies are approximately tuned [8]. Hence, for this device, it was not essential that the resonant frequencies of the B_{30}, B_{03}, and B_{22} modes were exactly the same.

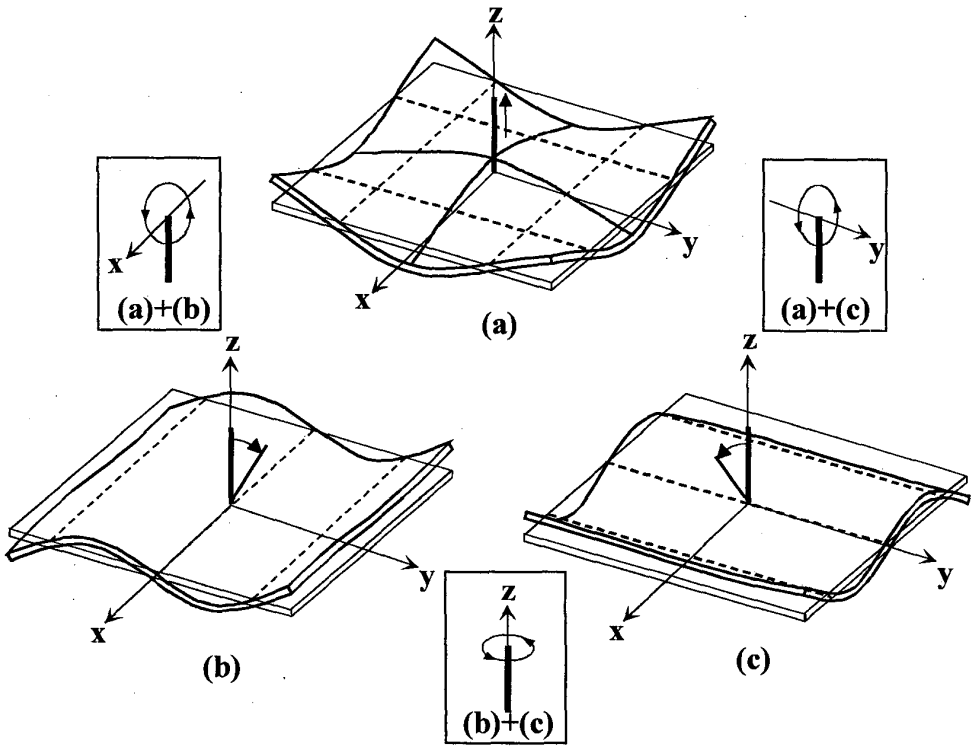

Fig. 2. Vibration modes. B_{22} mode, B_{30} mode, and B_{03} mode and their associated displacements at the center of the square plate and the relationships between the rotation direction and vibration combination (a, b, and c, respectively).

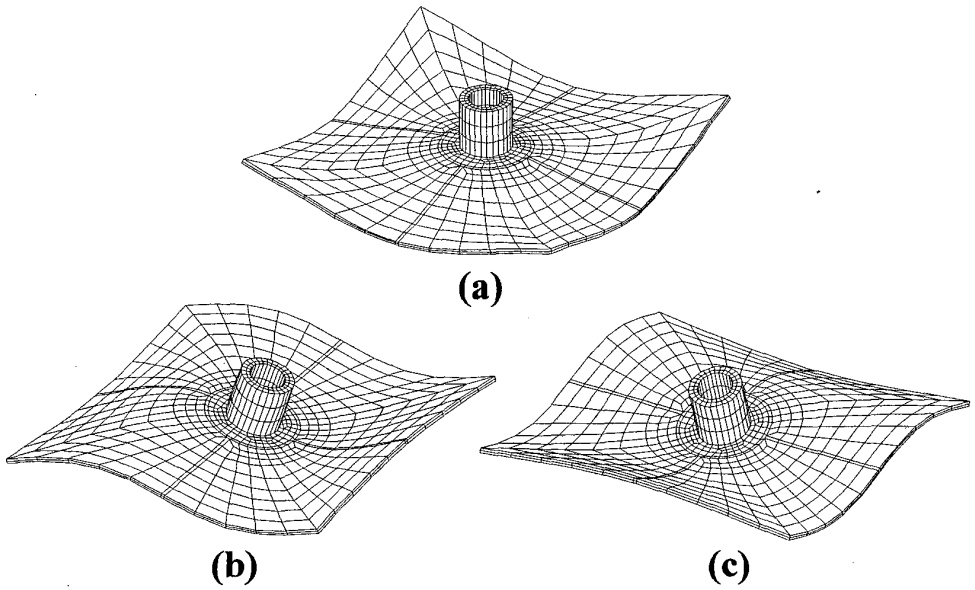

Fig. 3. Modal analysis results: a) B_{22} mode at 16.49 kHz, b) B_{30} mode, and c) B_{03} mode at 14.47 kHz.

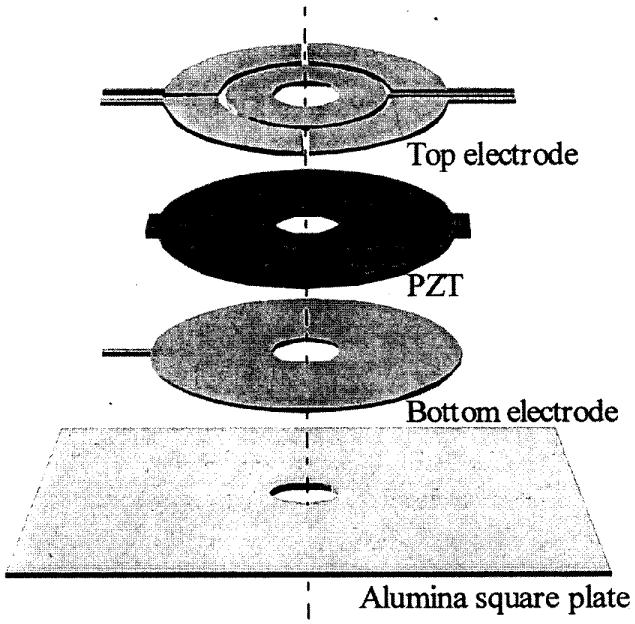

Fig. 4. Schematic of the arrangement of the electrode layers and PZT layer printed on an alumina substrate.

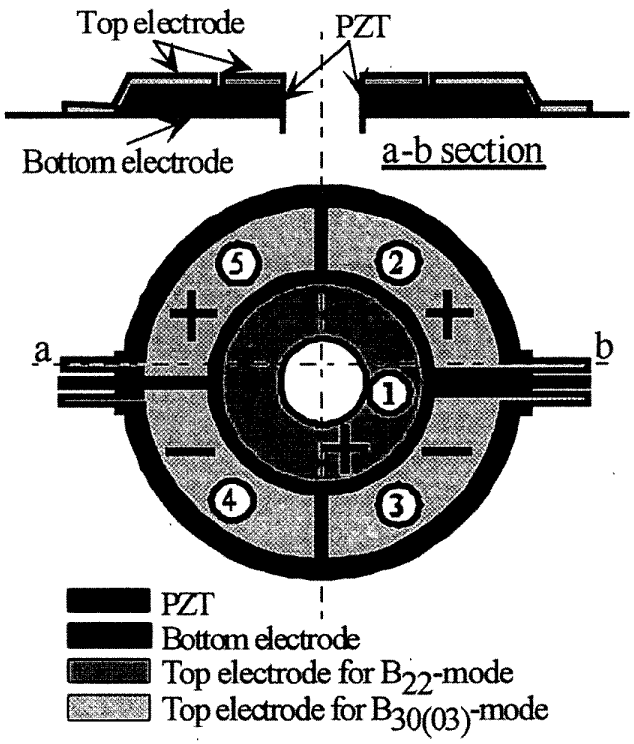

Fig. 5. Layout of the electrodes and the PZT layer. The direction of polarization is indicated by the plus and minus signs.

III. Fabrication and Experimental Procedure

A. Thick-Film Printed Layers

The first step in the fabrication process was to deposit the bottom electrode. This was achieved by screen printing the required pattern, a circular ring and leadout, at the center of the alumina substrate, as shown in Fig. 4. A gold cermet conductor (ESL 9336) was used for both top and bottom electrodes. The electrode was dried at 150°C and fired at 890°C to sinter the film. The PZT paste was made from 95% PZT-5H powder (supplied by Morgan Electroceramics Ltd.), 5% lead borosilicate powder, and organic vehicle (ESL 400). This paste was printed through a stainless steel screen with a 23-μm thick emulsion layer using a Dek 1750RS printer [12]. Two print strokes were used to deposit a film that was then dried and fired. This was followed by an additional triple print, dry, and fire process, which yielded a PZT thickness of 95 μm. The PZT film was sintered at 890°C. Next, the top electrode, patterned as shown in the upper part of Fig. 4, was printed onto the PZT and subsequently dried and fired as before. The PZT is deposited in a sandwich between the top and bottom electrodes, forming a capacitor structure. The layout of the thick-film printed PZT and electrodes, and a cross-section through the electrode/PZT/electrode sandwich, is illustrated in Fig. 5. The top electrode consists of one ring to excite the B_{22} mode and four quadrants to excite the B_{30} and B_{03} modes. To excite and control the B_{30} and B_{03} modes of operation, the PZT between the quadrants on opposite halves of the device must be poled in opposite directions. To achieve this, a dc bipolar voltage source was simultaneously applied to the top electrodes, generating a poling field of $\pm$4.2 MV/m on the appropriate electrodes. During poling, the PZT is maintained at 150°C. Finally, the alumina cylinder was bonded with an adhesive at the center of the plate. Photographs of the motor showing the alumina plate and cylinder and the thick-film printed PZT layers and electrodes are shown in Fig. 6. A stainless steel ball 3 mm in diameter is used as the rotor and is located on the cylinder.

B. Vibrator Performance

The resonant frequencies of the B_{30} and B_{22} modes were found, by measuring electrical impedance, to be 15.86 and 16.67 kHz, respectively. In this instance, the structure was excited by a driving voltage of 1 V rms. The frequency difference between the B_{30} and B_{22} modes was 1.2 kHz, and this was lower than the simulation result. The resonance responses were, however, rather small, and this is because the thick-film printed PZT layer has a relatively low piezoelectric coefficient, d_{31}, of approximately -33 pC/N compared with the bulk value of -274 pC/N [13].

Next, the structure was analyzed on a purpose-built optical fiber interferometer. Fig. 7 shows the amplitudes of displacement of each mode, and the phase difference between the applied signal and displacement, plotted against frequency. The applied excitation voltage for these measurements was 200 V, peak to peak. The resonant frequencies of the B_{30} and B_{22} modes were found to be to 15.45 and 16.2 kHz, respectively. This is again lower than

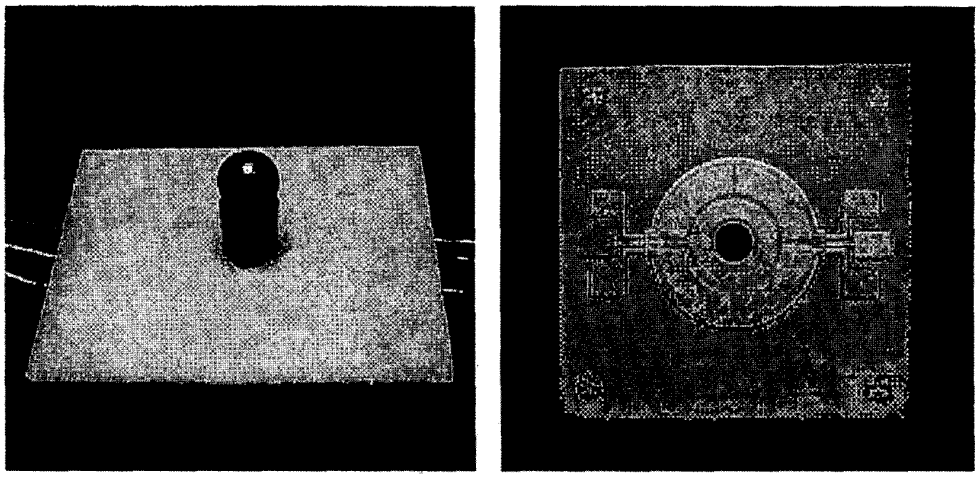

Fig. 6. Photographs of MDOF ultrasonic motor (a) and the surface of the thick-film printed PZT layer (b).

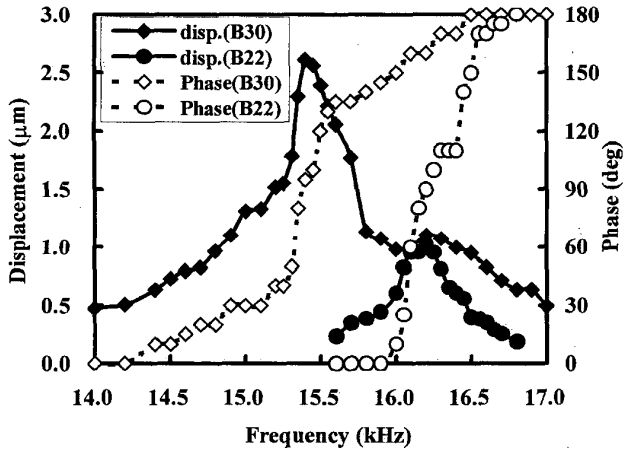

Fig. 7. Measured displacement and phase difference between applied voltage and displacement.

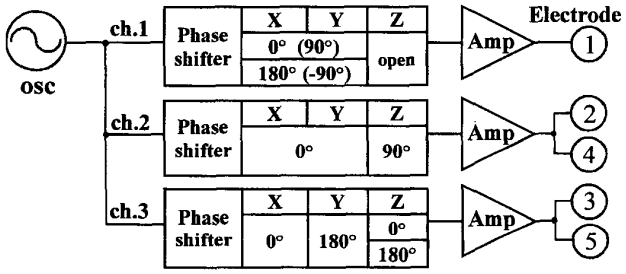

Fig. 8. Block diagram of the three-phase drive circuit for the MDOF ultrasonic motor.

the simulated values and also lower than the resonant frequency detected by the electrical impedance analysis described previously. This is because the optical interferometer measurements were taken with a much larger driving voltage, which increases the vibration velocity. This is due to the fact resonant frequencies fall with increasing vibration velocity.

Although the mode shape of each resonance was not fully mapped, the interferometer was used to confirm that the direction of vibration of the cylinder agreed with the design. The vertical displacement of the B_{22} mode at the end face of the cylinder was measured at resonance using the interferometer and found to be 1.1 μm. The motor was positioned sideways under the interferometer to enable the horizontal displacements of the B_{30} mode to be measured. The interferometer was positioned over the side face of the cylinder near the top edge. The horizontal displacement of the B_{30} mode was found to be 2.2 μm at its resonance frequency. The amplitude of the B_{30} mode was also found to be 1.2 μm at the resonance frequency of the B_{22} mode. This amplitude was sufficient to drive the rotor, and, therefore, the motor could only be operated near the resonance frequency of the B_{22} mode. The phase difference of the displacements of both modes varies with drive frequency. At the resonant frequency of the B_{22} mode, the phase difference between displacements of the B_{30} mode and B_{22} mode was approximately 90°. Hence, elliptic displacement motions for rotations around x- and y-axes occur when the drive signals for both modes are either in phase or out of phase.

C. Rotation Directions and Drive Circuit

This type of ultrasonic motor requires a three-phase drive source for its operation. Fig. 8 shows a block diagram of the drive circuit for the ultrasonic motor. The phase values in parentheses must be applied when each mode has the same resonance frequency. If the resonance frequency of the B_{22} mode is different from the others, the phase of channel 1 at rotations around the x- and y-axes has to be shifted. It was found that the phase difference of

channel 1 was zero because there was already a phase difference of 90° between the displacement of the B_{30} mode and the B_{22} mode. A signal from a function generator was split into three, and then each phase was adjusted with a phase-shift network to a value corresponding to a rotation direction. The adjusted signals were amplified up to 200 V peak to peak by amplifiers and then applied to each electrode. Changing the rotation axis was accomplished by toggling channel 1 and simultaneously switching the phase of channels 2 and 3. All electrodes were used for rotations around the x- and y-axes, and the rotation change between these was achieved by inverting the phase of the signal on channel 3, thus switching between the B_{30} and B_{03} modes. Moreover, by inverting the phase of channel 1, rotations around both axes were reversed. For rotation around the z-axis, channel 1 must be opened, and the phase difference between channels 2 and 3 should be adjusted to +90° or −90°. In this case, the phase of channel 2 is fixed at +90° and that of channel 3 is inverted for a reverse motion of rotation. Using this drive circuit, all directions of rotation were confirmed.

D. Velocity and Rotation Angle

To make a pre-load, the small metal spherical rotor of mass 0.1 g was put on the cylinder, as shown in Fig. 6(a). It was pulled down onto the cylinder by an electromagnet, which enabled adjustment of the force toward the center of the vibrator. In this case, the pre-load was equivalent to 0.86 g, including the weight of the rotor. A small metal pin was also attached to the sphere to enable measurement of angular displacement. The mass of the pin was negligible compared with that of the spherical rotor, and, therefore, its effects on the angular displacement of the rotor can be neglected. The angular displacement of the rotor was clearly indicated by the pin, and this enabled precise measurement using a suitable protractor. Rotation angles of the rotor were changed by applying short bursts containing a number of sinusoidal pulses with a frequency of 16.23 kHz and an amplitude of 200 V peak to peak, as illustrated in Fig. 9. Using this form of drive, measurements were then taken to determine the angular velocity and angular resolution achievable. An example of the measurement results is shown in Fig. 10. The average velocities were calculated by dividing the measured angular rotation by the duration of the burst of pulses. At least 10 pulses were required to start the motor running under this condition. For a small number of pulses, the angular velocity rapidly increased to a maximum value of approximately 20 rad/s. Once this velocity is reached, it remains steady and repeatable. The maximum angular velocity obtained is limited by the contact duration and vibration velocity of the device [14].

This method of driving the motor means the rotation angle can be determined by applying a given number of pulses, and, therefore, precision positioning of the rotor is possible. When the steady angular velocity region has been reached, the resolution of each angle was simply calculated

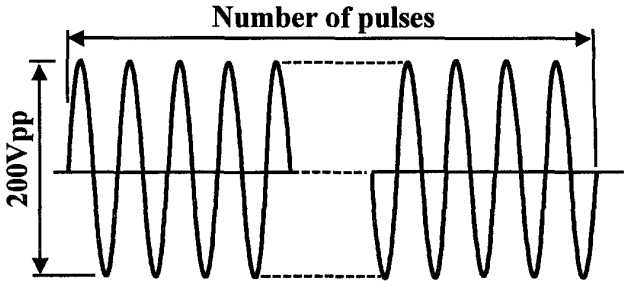

Fig. 9. Sinewave pulses of 16.23 kHz and 200 V_{pp} amplitude applied to the MDOF ultrasonic motor.

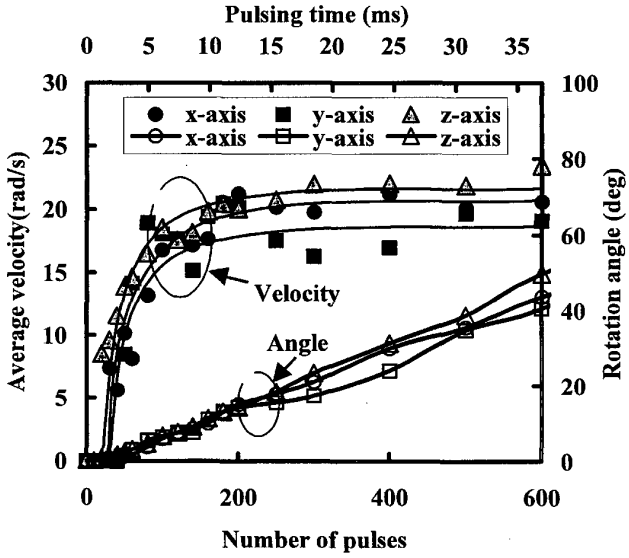

Fig. 10. Measured velocity and rotation angle driven by the signal shown in Fig. 9.

from rotation angles divided by number of pulses and was found to be 0.08 deg for the x-axis, 0.07 deg for the y-axis, and 0.087 deg for the z-axis per unit pulse. This level of resolution is only achievable if given very smooth and uniform contact surfaces. At present, the roughness of the contact surface between a rotor and stator means this level of resolution cannot be achieved in practice. However, it is also possible to achieve finer angular resolution by applying a burst of pulses of <5 ms duration, i.e., operate the device in the non-linear region. This approach is only feasible provided the behavior of the motor is repeatable in the non-linear region. Theoretically, the properties of both of the x- and y-axes should be the same. The experimental results, however, indicate a small difference between the two. The cause of this is probably that the conditions of the contact surfaces between the rotor and the cylinder were slightly different between both rotations. When the motor is in operation, the rotor and the cylinder are in contact at a small point so that motor performance is greatly affected by the surface condition. Therefore, factors such as, for example, temperature, humidity, and rough-

ness will influence the performance of the motor. Further studies are underway to improve the stability and increase the output torque.

IV. Conclusions

A MDOF ceramic ultrasonic motor comprising thick-film printed PZT layers has been successfully realized. The PZT layer generates enough force to obtain sufficient displacement for the motor to operate. This motor not only has a relatively simple structure, but also can produce rotations in three orthogonal directions, as confirmed by both simulated and experimental results. Further improvements to the contact surface uniformity would increase the stability of this motor and enable precision positioning of the rotor. Under such conditions, this device would be capable of a resolution of rotor angle of approximately 0.08 deg per unit pulse after the initial 5-ms burst of drive pulses. The possibility of improving this resolution and accuracy of the rotor positioning by operating the motor in the non-linear region (<5 ms) is also currently being investigated.

This work has verified that thick-film printed PZT layers are a relatively efficient method for driving an ultrasonic motor. Moreover, thick-film printed PZT technology will enable the reduction of manufacturing costs compared with other types of ultrasonic motors. One drawback, however, is that a high voltage source is needed for this type of ultrasonic motor because of the low piezoelectric activity of the thick-film PZT film. Ongoing work at Southampton is aimed at improving the piezoelectric properties of screen-printed films. This will help to improve the performance of the motor further.

Acknowledgments

The authors thank the staff of University of Southampton Institute of Transducer Technology for help with the PZT printing and device measurements. The assistance of T. Papakostas and N. Grabham are gratefully acknowledged. In addition, M. Aoyagi is grateful to Y. Tomikawa, Yamagata University in Japan, for granting an opportunity to study in the UK and receive a visiting research fellowship from the Ministry of Education, Science, Sports, and Culture, Japan.

References

[1] A. Iino, K. Suzuki, M. Kasuga, M. Suzuki, and T. Yamanaka, "Development of a self-oscillating ultrasonic micro-motor and its application to a watch," *Ultrasonics*, vol. 38, pp. 54–59, Mar. 2000.

[2] V. Tvarozek, I. Novotny, I. Cerven, J. Kovac, and T. Lacko, "RF reactive sputtering of zinc-oxide films on silicon and Si-SiO2-TiN substrates," *Sensors Actuators A-Phys.*, vol. 30, pp. 123–127, Jan. 1992.

[3] M. Sayer, D. Barrow, L. Zou, C. V. Vasant, R. Kumar, R. Noteboom, D. A. Knapik, D. W. Schindel, and D. A. Hutchins, "Piezoelectric and capacitive microactuators and devices," in *Mater. Res. Soc. Symp. Proc.*, pp. 37–39, 1993.

[4] K. Shimomura, T. Tsurumi, Y. Ohba, and M. Daimon, "Preparation of lead zirconate titanate thin-film by hydrothermal method," *Jpn. J. Appl. Phys.*, vol. 30, pp. 2174–2177, Sep. 1991.

[5] M. Koch, N. Harris, R. Maas, A. G. R. Evans, N. M. White, and A. Brunnschweiler, "A novel micropump design with thick-film piezoelectric actuation," *Meas. Sci. & Technol.*, vol. 8, pp. 49–57, Jan. 1997.

[6] W. D. Callister Jr., *Materials Science and Engineering, An Introduction.* 3rd ed. New York: John Wiley & Sons, 1994, ch. 20.

[7] H. Hata, Y. Tomikawa, S. Hirose, and T. Takano, "Ring-form two-dimensional (X-Y) moving piezoelectric actuator," *Jpn. J. Appl. Phys.*, vol. 35, pp. 5023–5026, Sep. 1996.

[8] S. Ueha and Y. Tomikawa, *Ultrasonic Motors—Theory and Applications.* Oxford: Clarendon Press, 1993, ch. 3.

[9] M. Aoyagi, T. Ogasawara, Y. Tomikawa, and T. Takano, "Multi-degrees-of-freedom ultrasonic actuator employing multi-vibration modes of a disk," in *Proc. 7th Int. Conf. New Actuators Germany (ACTUATOR 2000)*, pp. 399–402, 2000.

[10] T. Amano, T. Ishii, K. Nakamura, and S. Ueha, "An ultrasonic actuator with multi-degree of freedom using bending and longitudinal vibrations of a single stator," in *Proc. 1998 IEEE Ultrason. Symp.*, pp. 667–670.

[11] M. Kurosawa, K. Nakamura, T. Okamoto, and S. Ueha, "An ultrasonic motor using bending vibrations of a short cylinder," *IEEE Trans. Ultrason., Ferroelect., Freq. Contr.*, vol. 36, pp. 517–521, May 1989.

[12] N. R. Harris, S. P. Beeby, N. M. White, M. Koch, and A. G. R. Evans, "Thick-film printing of PZT onto silicon for micromechanical applications," in *Proc. Micromechan. Europe 1998 (MME'98)*, pp. 78–81.

[13] *Piezoelectric Ceramics Data Book for Designers.* UK: Morgan Matroc Ltd.

[14] K. Nakamura, M. Kurosawa, and S. Ueha, "Design of a hybrid transducer type ultrasonic motor," *IEEE Trans. Ultrason., Ferroelect., Freq. Contr.*, vol. 40, no. 4, pp. 395–401, Jul. 1993.

Manaba Aoyagi was born in Yamagata, Japan in 1966. He received the B.Sc. degree in electrical engineering in 1989 and the M.Sc. degree in 1991, both from Yamagata University, Yonezawa, Japan and the Ph.D. degree in 1998 from Tokyo Institute of Technology, Tokyo, Japan. He is currently a research associate in the Department of Electrical Engineering, Yamagata University, working on development of ultrasonic motors and piezoelectric actuators. He worked with the University of Southampton, U.K. as a visiting research fellow for a period of one year, September 1999 to September 2000. His current research interests are in the areas of powerful ultrasonic motors, microactuators, and multi-degree-of-freedom piezoelectric motors and actuators. He is a member of the Institute of Electronics, Information, and Community of Japan and the Acoustic Society of Japan. He received the Young Engineer Award in 1994 and the Awaya Young Engineer Award in 1997 from both societies just mentioned, respectively.

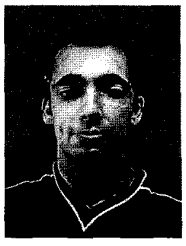

Steve Beeby obtained his BEng (Hons) in mechanical engineering in 1992 and was awarded his PhD in 1998. He is currently a research fellow in the Department of Electronics and Computer Science and is researching in the field of microelectromechanical systems (MEMS). In particular, his research involves the development of fabrication processes whereby thick-film piezoelectric materials can be combined with micromachined silicon structures. This work is the first of its kind. To demonstrate the feasibility of this

approach, he has designed and fabricated an accelerometer and resonator using this combination of technologies. He is also involved in an industrially funded research project investigating the application of a micromachined silicon resonator for strain-sensing applications. He has also designed and fabricated a micromachined silicon capacitive pressure sensors for a variety of pressure ranges. His skills include the finite element modelling and design of MEMS devices, silicon processing and MEMS packaging, and testing. Future research interests include the development of ultrasonic devices (a particle filter and flow sensor) for microfluidic applications and a silicon microphone. Both devices will be realized using thick-film piezoelectric layers on silicon. Steve currently has over 40 publications in the field and has co-authored several successful proposals to both industry and the EPSRC.

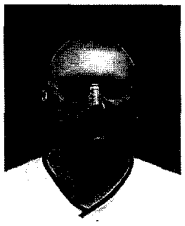

Neil M. White received the PhD degree from the University of Southampton, UK in 1988. He was appointed Lecturer in 1990 and is currently Reader within the Department of Electronics and Computer Science, University of Southampton. He is also Research Director of the University of Southampton Institute of Transducer Technology (USITT). He has published extensively in the areas of thick-film sensors and intelligent instrumentation and is author or co-author of over 70 academic publications, including the monograph *Intelligent Sensor Systems*. Dr. White is both a Chartered Engineer and Chartered Physicist in the UK and is a past Chairman of the Instrument Science and Technology Group (ISAT) of the Institute of Physics (IOP).